Influence of Ductility on the Performance of Lunar Habitat Structures under Recurrent Disturbances

Arsalan Majlesi *
The University of Texas at San Antonio, San Antonio, Texas 78249

Amir Behjat †
Purdue University, West Lafayette, Indiana 47906

Adnan Shahriar‡
The University of Texas at San Antonio, San Antonio, Texas 78249

Hamid Khodadadi Koodiani§
The University of Texas at San Antonio, San Antonio, Texas 78249

Shirley J. Dyke ¶
Purdue University, West Lafayette, Indiana 47906

Julio Ramirez ‖
Purdue University, West Lafayette, Indiana 47906

Arturo Montoya **
The University of Texas at San Antonio, San Antonio, Texas 78249

This research examines how ductility affects the durability of lunar surface structures against recurring disturbances like moonquakes, micrometeorite impacts, and thermal cycles, over an extended period. The structural performance at various levels of ductility was determined by adjusting material parameters and thickness of a reference multilayered dome structure. Moonquake and micrometeorite impact-induced lateral displacements were estimated using a Reduced Order Model (ROM) under a Control-oriented Dynamic Computational Modeling (CDCM) framework. The study considered the degradation of the metallic dome's strength properties over time due to thermal cycles. Fragility curves were generated by assessing the likelihood of reaching three predefined damage levels as a result of multiple hazards. Additionally, a discounted cash flow analysis was conducted to incorporate a financial aspect in the performance comparison. The findings revealed that structures with sufficient ductility capacity have a lower probability of sustaining severe damage or collapsing within a shorter

*Research Assistant, School of Civil & Environmental Engineering, and Construction Management
†Postdoctoral Researcher, School of Mechanical Engineering, and AIAA member
‡Research Assistant, Department of Mechanical Engineering
§Research Assistant, School of Civil & Environmental Engineering, and Construction Management
¶Professor, Lyles School of Civil Engineering and School of Mechanical Engineering
‖Professor, Lyles School of Civil Engineering and School of Mechanical Engineering
**Professor, School of Civil & Environmental Engineering, and Construction Management, and Department of Mechanical Engineering [Corresponding Author]

time-frame. Hence, having ductile structures in lunar environments is advantageous as it allows the postponement of maintenance and repair actions, thereby conserving scarce resources for more urgent tasks. Moreover, the financial analysis demonstrated that lunar habitats with higher ductile capacities result in larger net present values, offering a higher return on the initial investment.

Nomenclature

b	=	material constants for the strain-life curve
C	=	ratio of dynamic to static strength under single time loading
C_f	=	coefficient to account the influence of load change frequency on fatigue strength
C_I	=	initial cost, $
C_{LC}	=	life-cycle cost, $
C_{trans}	=	cost of transportation, $/kg
c	=	material constants for the strain-life curve
d	=	design configuration
E	=	modulus of elasticity, MPa
$ENPV$	=	expected net present value, $
f	=	effective dose function, mSv/day
f_c	=	compressive strength of regolith, MPa
f_{cy}	=	loading frequency, Hz
f_c^f	=	fatigue strength of regolith under compression, MPa
g	=	limit state function
H'	=	material constant for the strain-life curve
h	=	total thickness of dome, cm
LD	=	lateral drift
M_A	=	mass of material A, kg
MDI_i	=	mean damage index of the ith damage state
N	=	number of loading cycles
NPV	=	net present value, $
n'	=	material constant for the strain-life curve
P_i	=	internal pressure, Pa
P_i^p	=	probability of passing damage state i

$P_\circ$ = external pressure, Pa

$RNPV$ = standard deviation of net present value, $

R_{str} = radius of the dome, m

T_i = internal temperature, K

$T_\circ$ = external temperature, K

t = time, day

t_{al} = thickness of aluminum, m

t_{re} = thickness of regolith, m

t_{st} = thickness of steel, m

v = value of design configuration, $/hr

X_t = state at time t

β = discount factor

Δ = roof displacement of the dome, m

Δ_{max} = maximum roof displacement of the dome, m

Δ_y = displacement at the elastic limit, m

ε_a = strain amplitude

$\varepsilon_f^{'}$ = true fracture strain

λ = annual discount rate

ρ_{al} = density of aluminum, kg/m^3

ρ^f = cycle asymmetry coefficient

ρ_{re} = density of regolith, kg/m^3

ρ_{st} = density of steel, kg/m^3

σ_a = stress amplitude, Pa

$\sigma_f^{'}$ = fracture strength, MPa

σ_{cr} = critical stress, MPa

σ_i = level of fracture initiating stress, MPa

σ_m = mean stress for cyclic loading, MPa

σ_{max} = equivalent to the updated ultimate strength, MPa

σ_c^{max} = maximum cyclic stresses resulting from σ_z, MPa

σ_c^{min} = minimum cyclic stresses resulting from σ_z, MPa

σ_r = radial stress, MPa

σ_y = yield stress of material, MPa

σ_z = axial stress, MPa

σ_θ = hoop stress, MPa

I. Introduction

RECENT improvements in the launching of spacecraft increase the viability of transportation of humans to space and their long-term presence on the Moon [1–4]. However, the structural requirements for lunar design concepts are yet to be fully established [5–12]. At early stages of design, trade studies can become critical in identifying the structural characteristics that lunar habitats should possess to resist the harsh environmental conditions in space [13–15]. In addition, it would be logical to leverage the knowledge and best practices acquired in designing Earth structures resistant to extreme events, such as earthquakes and hurricanes.

Ductility is an important structural concept in seismic design for Earth structures, which describes their ability to undergo large-amplitude deformations without collapsing [16–18]. The seismic design philosophy has been shaped by the possibility of using the inelastic capacities of structures during seismic events, as it allows structures to resist large lateral force demands while guaranteeing life safety. Structures are designed to have sufficient ductile capacity to survive extreme loading event scenarios that can occur at the site during a specified return period [19, 20]. Although ductility is a relevant concept for Earth structures, its influence on the structural performance of future lunar habitats is unknown as the loading characteristics in space vary significantly from those on Earth.

During the Apollo program, the Apollo Passive Seismic Experiments (APSE) collected seismic activity from four stations network [21]. The seismic data were accumulated and sent back to Earth from 1969 to 1977 [22]. According to their source type, these seismic events were labeled as deep, thermal, and shallow moonquakes [22]. During this time, more than 12,500 moonquakes were registered and 28 of them were labeled as shallow moonquakes with a moment magnitudes close to 4.1 [23–25]. In a study conducted by Ruiz et al. [26], the seismic hazard on a lunar structure was computed considering only shallow moonquakes, as these are the most likely to cause damage to a lunar habitat [27–29].

Micrometeorites are another important hazard of the lunar environment that could introduce lateral displacements to future habitat structures [12, 30, 31]. On average, the Earth's path intersects with 33 tons of meteoritic material daily, most of which are micrometeorites that vanish at the Earth's atmospheric layer [32, 33]. Unlike Earth, the Moon cannot stop these micrometeorites from impacting the lunar surface. The Lunar flux model developed by Grun [14] estimates that a particle with a mass equal to 1 μg could interact with the lunar surface at an average of 2 $\frac{1}{\text{m}^2.\text{year}}$. The Grun Lunar flux model shows that the estimated Lunar flux reduces rapidly when increasing the micrometeorite mass, indicating that smaller micrometeorites are more likely to impact the lunar surface than larger micrometeorites. These particles range between 1–3 mm in size and can impact the lunar surface with an average velocity of 20 km/s; however, their velocity could reach up to 70 km/s [33].

Moreover, the high-temperature fluctuations on the lunar surface introduce cyclic thermal stresses, resulting in the long-term degradation of the utilized materials for lunar habitats. The temperature changes recorded during the Apollo landing sites varied from -171 C to 111 C [1]. A future lunar habitat will also interact with the thermal and pressure control systems that create a suitable living environment for humans, but also provide loading demands on the structure [34]. The interior temperature and pressure are expected to be adjusted during the crewed and dormant periods of the habitat.

Due to the characteristics of the loads in space, an evaluation of potential structure alternatives for lunar habitats requires conducting dynamic, multi-physics simulations that are inherently computationally expensive. Moreover, the loading inputs of these models are uncertain and have dependencies. Trade studies can ease the initial-decision making process and narrow down different system configurations for further in-detail analysis [35]. NASA has used trade studies as an initial decision-making tool to assess different system configurations for several missions [36–40]. Traditionally, they have had two approaches [41]: (i) comparing the advantages and disadvantages of a variety of alternatives; and (ii) using ranking systems based on different criteria and a weighting system. However, these two approaches do not capture essential elements for the evaluation of space habitats, as they do not account for (i) the physics of the problems; (ii) evolution of the system through time; (iii) interconnected systems; and (iv) uncertainties.

Recently, the CDCM framework was proposed as an alternative approach for conducting trade studies. The CDCM is a modular and computational efficient network for modeling system of systems, such as deep space habitats [42–44]. The framework was developed to provide the ability to run simulations that incorporate multiple disruptions and disturbances, experience damage and degradation, capture consequences over extended periods, and model repair and recovery efforts. Behjat et al. [43] used the CDCM to determine an appropriate maintenance period for a building experiencing both corrosion degradation and random moonquake events over its lifetime and selecting the most appropriate power generation and storage configuration for a lunar habitat exposed to solar radiation, dust, micrometeorite strikes, and exterior temperature fluctuations. The illustrative examples demonstrated that the CDCM can effectively address fundamental research questions related to the design of lunar habitats and their initial decision-making processes, particularly in the context of interconnected systems of systems with complex dynamics.

In the literature review performed for this paper, it was found that there is a lack of studies investigating the effects of moonquakes, and there is a notable absence of research exploring the combined and interactive effects of thermal fatigue, moonquakes, and micrometeorites on a lunar habitat throughout its lifespan. Thus, this paper employed the CDCM [42] to determine the influence of ductility on the performance of lunar habitat structures subjected to multiple disturbances, including moonquakes, micrometeorite impacts, and high thermal fluctuations. Following the systems of systems modeling approach of the CDCM, a structural subsystem was allowed to deform and deteriorate based on inputs received from the disturbance and interior environment subsystems of the habitat. The modeled structures were based on a simple two-layer design concept consisting of a metallic dome covered by a structural protective layer assumed to

be located as the same location where the Apollo 17 program was performed. The design provides adequate protection against radiation and prevents breaching of the structure due to micrometeorite impact. This design concept was selected due to its flexibility of adjusting its ductile capacity with minor modifications, which facilitates assessing if the ability of withstanding large plastic deformations before collapsing could provide potential benefits to the crew safety, daily space habitat operations, and maintenance activities.

The remainder of this paper is organized as follows. Section 2 provides the methodology followed to assess the performance of structures with varying ductility, including a description of the development of the structural model embedded within the CDCM. Section 3 describes the list of structures and performance metrics that were considered in the study. Section 4 contains the results of the trade study, including accumulated plastic deformation, fragility curves, and net present value for each of the structures. Section 5 discusses the potential impact of the results and the limitations of the study. Finally, Section 6 concludes with a summary of the lessons learned.

II. Methodology

Evaluating the influence of ductility on the performance of lunar structures requires estimating the damage due to recurrent disturbances over an extended period, defined as 20 years in this study. Due to the random nature of the disturbances, the loads applied to the structure should be probabilistic and capture the amplitude and recurrence intervals of the typical loads on the lunar surface, i.e., moonquakes and micrometeorite impacts. A long-term evaluation requires accounting for the degradation mechanism of materials exposed to large thermal cycles. In addition, since the trade study requires the evaluation of multiple structures with varying ductility capacities, the damage estimates must be obtained efficiently by running mechanics-based models that can provide rational damage approximations at a low computational cost. This section describes the tools and techniques employed in this research work.

The CDCM [42] was used as the framework to conduct the trade study. The CDCM's architecture provides the opportunity to conduct rapid simulations involving systems of systems models. The habitat system was assumed to include a core set of crucial subsystems, shown in Figure 1, to perform the structural assessment required in this study. This compact simulator included a structural subsystem and an interior environment subsystem.

The interior environment subsystem simulates the temperature and pressure inside the habitat. The habitat was assumed to be susceptible to different disturbances: (i) solar radiation; (ii) moonquakes; (iii) micrometeorite impacts; (iv) and exterior temperature fluctuations. The structural subsystem received the input from these blocks and estimated the response and damage due to the applied load. Additional details about the structural subsystem can be found in the subsequent section.

The CDCM integrated probabilistic models devised by by SanSoucie et al. [45] and Zook [46] to assess micrometeorite mass, diameter, and velocity within a given area. By establishing selected probabilities of exceedance and return periods, the expected characteristics of micrometeorites over a designated time frame were determined.

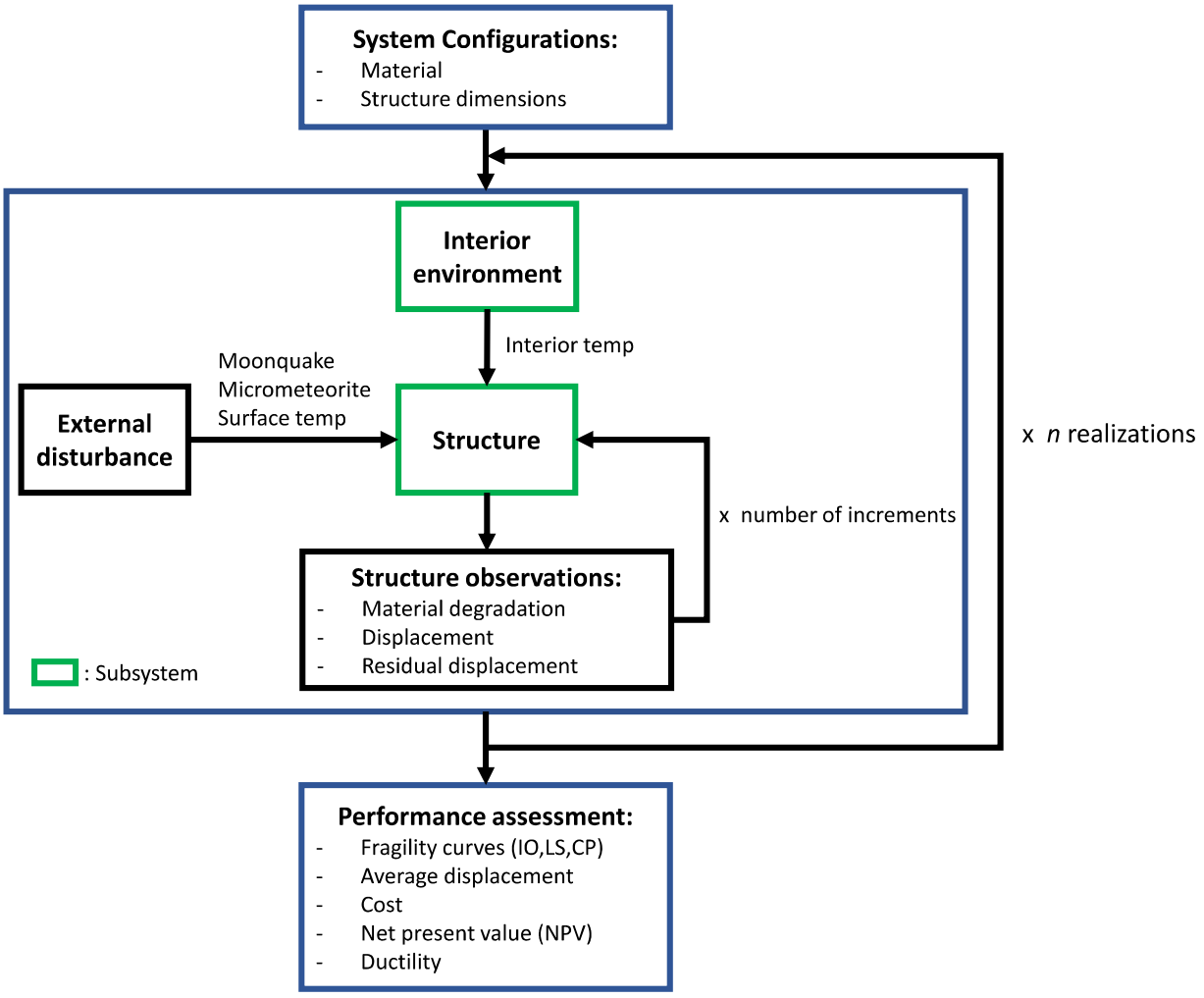

Fig. 1 Diagram of the lunar habitat system showing interactions between subsystems in the CDCM.

Moreover, the frequency of occurrence of moonquakes and their magnitudes were computed by the CDCM using probabilistic equations provided by Ruiz et al. [26].

A. Structural subsystem

1. Conceptual Design

The lunar habitat was assumed to be a monolithic dome structure covered by a regolith protective layer. This design concept was selected as the ductile capacity of the structure can be easily varied by adjusting the dome material and its thickness. All the dome structures under consideration had a thickness that ensured adequate protection against radiation and prevented full penetration of a micrometeorite impact.

According to Valentin [47], a human's body should not receive more than 50 mSv of radiation for extended exposures. NASA plans for astronauts to stay on the lunar surface for 2 months [48]. Thus, under a 2-month stay duration, an

astronaut can receive 0.83 mSv/day. NASA has released an On-Line Tool for the Assessment of Radiation in Space (OLTARIS) that allows users to download information on the radiation dose as a function of thickness for different materials [49–54]. OLTARIS was used to generate the curve shown in Figure 2 for lunar regolith. This tool provides radiation dose predictions using nuclear transport methods based on the HZETRN2005 dose equivalent algorithm [55, 56], which has been validated against measurements taken at the International Space Station (ISS) and the Space Shuttle program . It can be observed from Figure 2 that the overall trend is that the effective dose decays as a function of thickness, but it increases when the thickness ranges between 500 and 2,000 kg/m^2. This peak radiation phenomenon has also been observed in the Earth's atmosphere, and it is known as the Regener-Pfotzer maximum. This behavior indicates that secondary particles and photons produced due to cosmic rays are more intense at the entrance of the atmosphere. In accordance with Slaba [52], beyond 2,000 kg/m^2, exposure is primarily influenced by nucleons, pions, muons, and electromagnetic components.

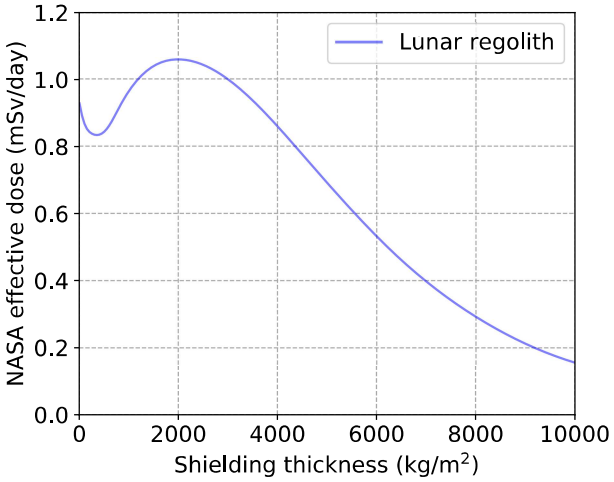

Fig. 2 Effective dose versus shielding thickness on the lunar surface [49–54].

In this study, the regolith protective layer was assumed to shield the structure against radiation. Thus, to receive a radiation dose of less than 0.83 mSv/day, the regolith layer must satisfy the following criterion in Eq. (1).

$$f(\rho_{re} t_{re}) \leq 0.83 \tag{1}$$

where function f is the lunar regolith curve shown in Figure 2, ρ_{re} is the density of the regolith shielding and t_{re} is the thickness of the regolith shielding.

Micrometeorite impacts also play an important role in the initial design of lunar habitats. As discussed previously, these particles range between 1–3 mm in size, and their velocity could reach up to 70 km/s [33]. Additionally, as stated by Allende [57], the perforation of the regolith shielding could reach up to 30 cm. Hence, if regolith is utilized as the exterior shielding, the initial design of a lunar habitat must also satisfy the following criteria.

$$t_{re} \geq 0.3 \tag{2}$$

2. ROM system

The performance of the lunar habitat structures was predicted using an ROM to allow efficient modeling of their response due to moonquakes, micrometeorite impacts, and thermal stresses. A Finite Element (FE) model was developed in OpenSees [58, 59] to allow rapid estimates of the response of the structures of interest within the CDCM platform. In this study, the ROM should capture the behavior at the lateral displacement of a multilayered dome due to moonquakes and micrometeriote impacts, as shown in Figure 3. The model should also account for the multiple layers of the dome shown in Figure 4. To capture the behavior at the tip of the dome, it was concluded that the dome structure could be represented as a single cantilever column carrying a mass equal to the weight of the structure, as shown in Figure 5. The model included 3 beam-column elements and 4 nodes and the mass was placed at node 3. Each node had 3 degrees of freedom, i.e., two translations in the xy plane and the rotation about the plane's normal. The location of the mass was determined by calculating the center of mass of a hollow hemisphere, which is at a distance equivalent to $R_{str}/2$ from its base, where R_{str} is the radius of the dome.

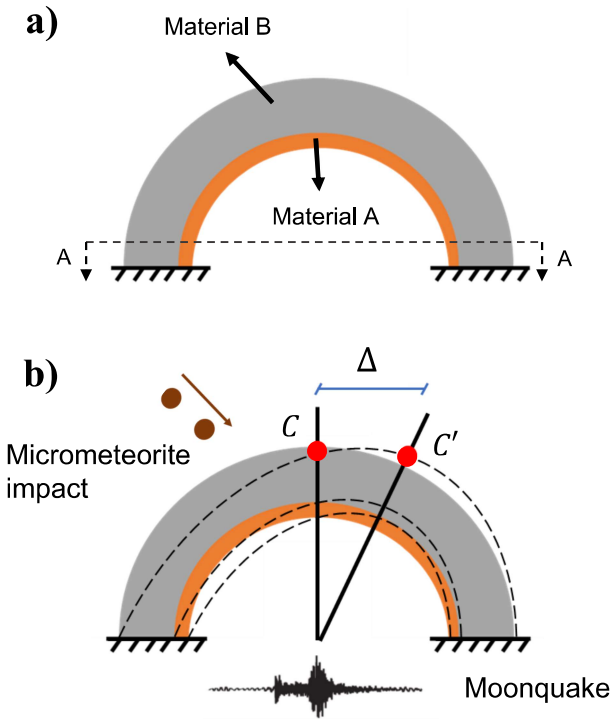

Fig. 3 Two layer dome structure: a) before lateral displacement applied; and (b) after lateral displacement applied.

The plastic deformation in domes typically occurs in areas nearer to the fixed base; thus, it was assumed that element

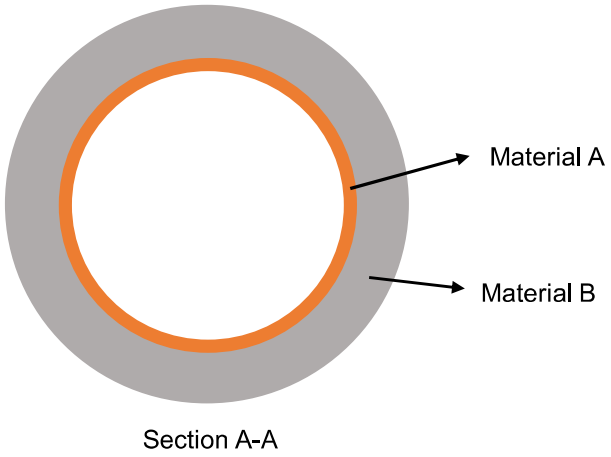

Fig. 4 The bottom cross section of the ROM system (A-A).

1 would behave as a nonlinear beam-column undergoing plastic deformation. The length of this element was chosen based on the recommendations provided by Ruangrassamee and Kawashima [60]. The nonlinear element was modeled using fiber-based nonlinear elements, as shown in Figure 5. The fiber section consists of divided patches of materials A and B, which were modeled using predefined materials Steel02 and Concrete02 [58], respectively. Elements 2 and 3 were assigned rigid beam-column to capture the general stiff behavior of the dome.

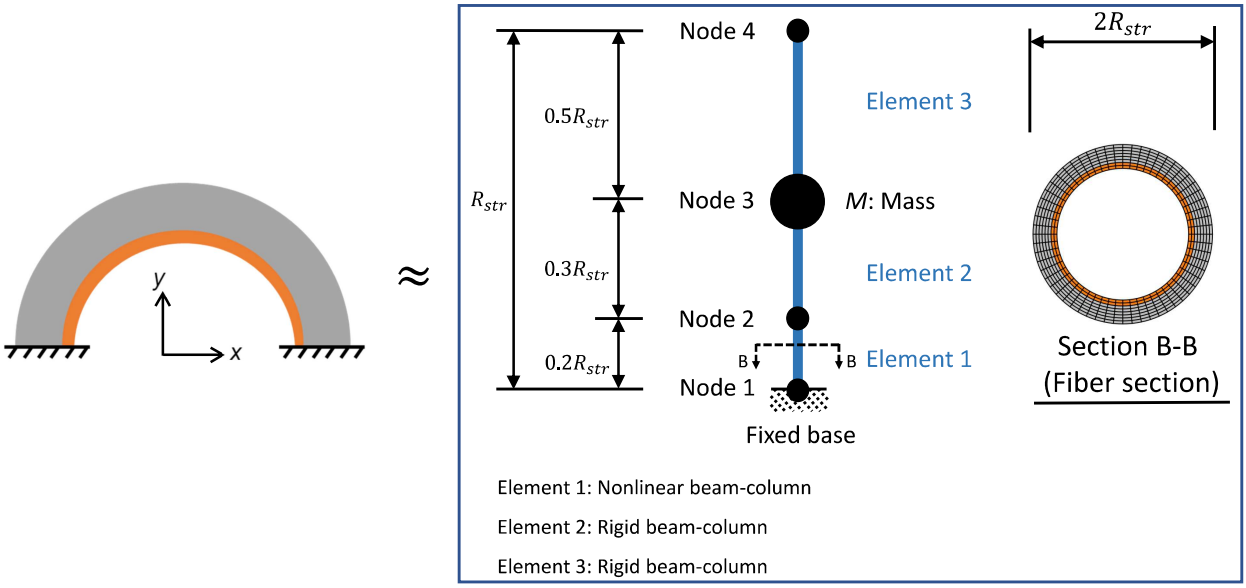

Fig. 5 Equivalent ROM cantilever column.

The verification of the ROM model was conducted by comparing the force-displacement curve obtained from a pushover analysis against the results of the same analysis performed on a high-fidelity model. A three-dimensional FE model of a multilayered dome composed of a 3 cm thick structural layer made out of steel with a yield stress of 248 MPa covered by a 120 cm structural protective layer made out of regolith with a compressive strength of 25 MPa was

analyzed using the commercial FE software ABAQUS [61]. The analysis was conducted using two steps: (i) in the first step, reduced gravity (1/6 g) was applied to the structure; and (ii) in the second step, a lateral displacement was applied to the tip of the dome. The structure was discretized using 8-noded linear brick elements with reduced-integration (C3D8R), which had dimensions smaller than 0.2 m. The lateral displacement of the 3D dome model is illustrated in Figure 6. A reasonable agreement was observed between the ROM and 3D model, as shown in Figure 7. This accuracy level is sufficient to perform a comparison between the performance of structures with different levels of ductility.

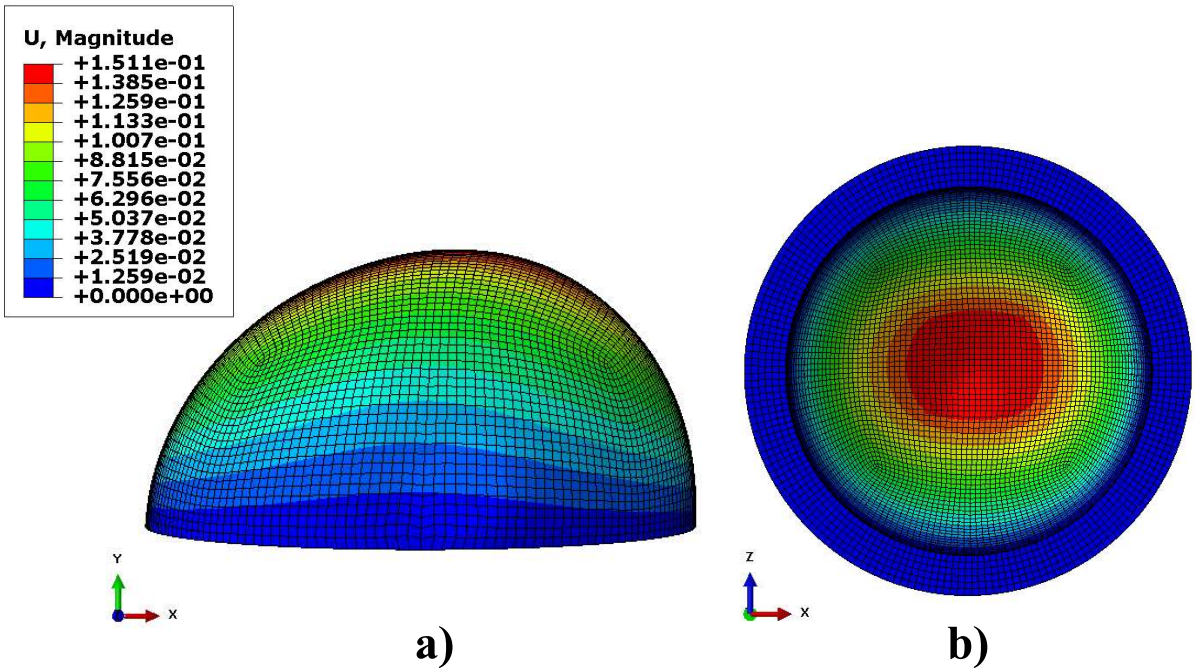

Fig. 6 Deformed shape of the dome (S3S248): a) side view; and b) bottom view.

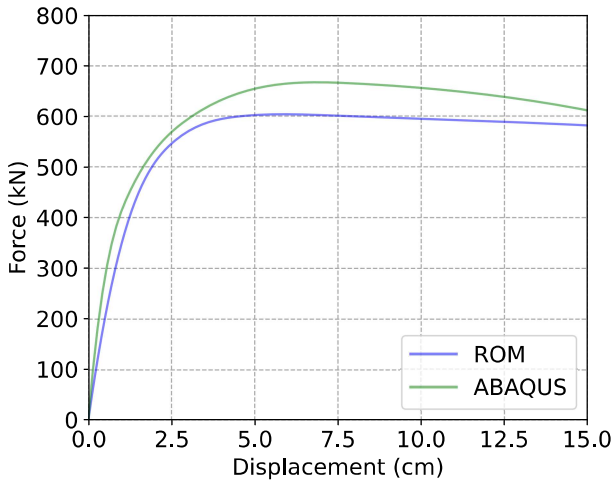

Fig. 7 Pushover curve comparison between a 3D Model and an ROM.

The displacement in the x-direction resulting from a moonquake on the ROM system was estimated using the algorithm provided by Fajfar [62]. This algorithm combines the pushover analysis of an ROM system with its response spectrum analysis. Moreover, in this method, the inelastic spectra with equivalent damping and period are utilized. Additional details for extracting the displacement demands are given in Appendix A.

To further proceed with this algorithm, the main frequency of the structures were extracted using the three-dimensional shallow spherical formulations provided by Kang [63]. This formulation can be employed to estimate the domes' frequencies as the structures meet the thick-walled spherical bodies criterion defined below, [64]:

$$0.2 < h/R_{str} \leq 0.5 \tag{3}$$

where h is the total thickness of the dome.

The displacement of the ROM system due to micrometeorite impact was captured by matching the kinetic area of the impact with the area underneath the pushover curve. The kinetic energy of a micrometeorite impact is dependent on the horizontal velocity and the size of the particle.

B. Thermo-mechanical stresses in a multilayered composite

The temperature gradient through the depth of the two layers of the structure was captured in the analysis. This temperature gradient introduces thermo-mechanical stresses to the structure that contribute to the performance of the structure under external disturbances. An analytical solution based on thermo-elasticity theory [65] was utilized for estimating the stress distribution of the two-layered dome subjected to an internal pressure and a thermal load. The analytical solution takes the internal temperature (T_i), external temperature ($T_\circ$), internal pressure (P_{int}) and external pressure ($P_\circ$) into account and the resulting outputs are the radial stress (σ_r), hoop stress (σ_θ) and axial stress (σ_z), as shown in Figure 8. In this study, it was assumed that σ_r and σ_θ are negligible; therefore, the variation of σ_z as a result of high temperature fluctuations was the only source for material degradation. The equations provided in the following section, take σ_z as an input for cyclic stresses.

C. Material degradation

The cyclic temperature fluctuations in the design of a lunar habitat degrade the structural materials. Thus, the long-term performance of these structures must consider potential fatigue failure of the structural materials. The ultimate strength of the implemented materials were updated annually in the CDCM (structural subsystem) based on the cyclic thermal stresses (σ_z) as discussed in the previous section. Therefore, strength reduction was applied to the utilized materials in element 1 of the equivalent ROM models which also created updated pushover curves by the end of each year. In this case, the lateral displacements caused by moonquakes and micrometeorite impacts were computed based on the updated pushover curves. The following assumption enabled the CDCM to be computationally efficient while

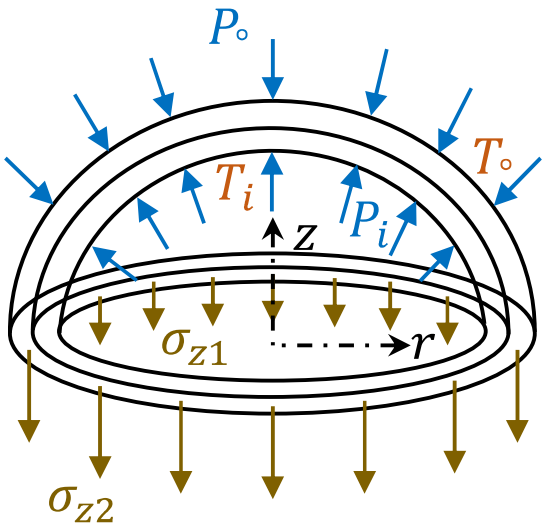

Fig. 8 Sketch of stress distribution for a two layer dome.

also taking the material degradation into account. The ultimate strength of the implemented materials were updated based on the following formulations.

Regolith [66]:

The fatigue strength of regolith was based on the formulations provided by Hola [67].

$$f_c^f / f_c = CN^{-A}(1 + B\rho^f \log N)C_f \tag{4}$$

where f_c^f is the fatigue strength of regolith under compression, f_c is the compressive strength of regolith [68], C is the ratio of dynamic to static strength under single time loading, N is the number of loading cycles, ρ^f is the cycle asymmetry coefficient, σ_c^{min} and σ_c^{max} are the minimum and maximum cyclic stresses resulting from σ_z, C_f is a coefficient to account the influence of load change frequency on fatigue strength, and A and B are coefficients.

The cycle asymmetry coefficient ρ^f is defined by the following equation:

$$\rho^f = \sigma_c^{min} / \sigma_c^{max} \tag{5}$$

Coefficient C_f is described by:

$$C_f = 1 + 0.07(1 - \rho^f) \log f_{cy} \tag{6}$$

where f_{cy} is the loading frequency (Hz) and A and B are calculated as below:

$$A = 0.008 - 0.118 \log(\sigma_i / f_c) \tag{7}$$

$$B = 0.118(\sigma_{cr}/\sigma_i - 1) \tag{8}$$

where σ_i is the level of fracture initiating stress and σ_{cr} is the critical stress.

Aluminum and steel:

The fatigue strengths of aluminum and steel were based on the modified Morrow approach [69]. To obtain the strain amplitude ε_a, the following equation was utilized:

$$\varepsilon_a = \frac{\sigma_f^{'}}{E}(1 - \frac{\sigma_m}{\sigma_f^{'}})(2N_f)^b + \varepsilon_f^{'}(2N)^c \tag{9}$$

where b and c are material constants for the strain-life curve [70], E is the modulus of elasticity, $\sigma_f^{'}$ is the true fracture strength, σ_m is the mean stress for cyclic loading (estimated from σ_z in the previous section), $\varepsilon_f^{'}$ is the true fracture strain and N is the number of load cycles. The stress amplitude, (σ_a), can be derived by solving Eq. (9),

$$\varepsilon_a = \frac{\sigma_a}{E} + (\frac{\sigma_a}{H'})^{1/n'} \tag{10}$$

where H' and n' are material constants for the strain-life curve [71]. Finally, the maximum stress endured in the cyclic loading can be obtained,

$$\sigma_{max} = \sigma_m + \sigma_a \tag{11}$$

where σ_{max} is equivalent to the updated ultimate strength of the degraded metallic alloy.

D. Damage levels

The ROM will provide displacement approximations of the lunar habitat under micrometeorite impacts and moonquakes. A criteria must be established to determine the damage levels as a function of the deformations experienced due to the applied disturbances. Hence, the Lateral Drift (LD) was evaluated during the loading of the structures. LD is defined as below:

$$LD = \frac{\Delta}{R_{str}} \tag{12}$$

where Δ is the displacement of the roof of the structure, as shown in Figure 3, and R_{str} is the radius of the dome. This study leveraged the damage states defined by FEMA 356 [72] to assess the impact of the loading on the integrity of

the structure [73]. FEMA 356 defines 3 different damage levels along the force-LD curve as shown in Figure 9, which are:

- Immediate Occupancy (IO): Structure is considered safe to occupy after event but likely not useful until rehabilitation performed.
- Life Safety (LS): Structure is safe during event but possibly not afterwards.
- Collapse Prevention (CP): Structure is on the verge of collapse and possibly total loss.

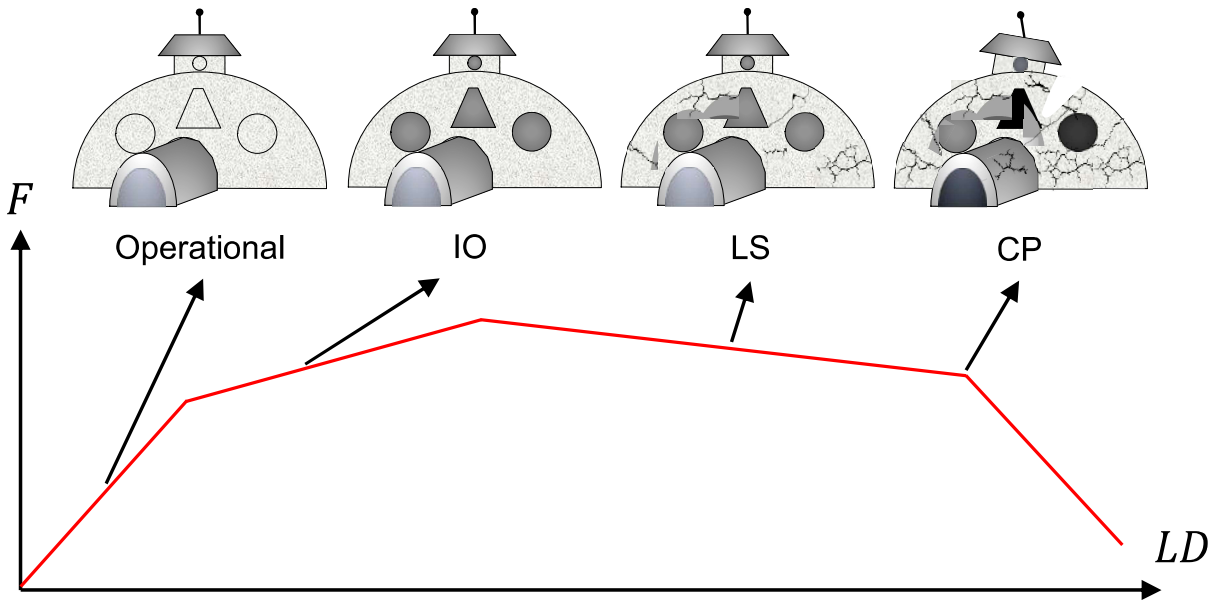

Fig. 9 Damage levels defined by FEMA 356 [72].

In the IO state, the structure has experienced minor cracks on non-structural instances. In the LS level, the structure has moderate damage and residual strength with permanent drift. While in the CP level, the structure has experienced severe damage, but has a minimal strength remaining in it [74]. Based on the various drift limits provided by FEMA 356, the performance of a structure is presented in Table 1.

Table 1 Drift limits at various performance levels [72].

Performance level	LD limit (%)
IO	1.0
LS	2.0
CP	4.0

III. Trade study

The trade study analyzed eighteen structures with different configurations and ductile capacities. Table 2 shows the six types of metallic alloys that were considered for the first layer and the lunar regolith assigned to the outer layer. The thickness of the inner layer varied from 1 to 10 cm, whereas the thickness of the outer layer was kept constant (120

cm) for all cases. All eighteen structural designs satisfied the conditions defined by Eqs. (1) and (2). These design considerations control the depth of the layers and alter their ductility. Moreover, the ductility factor ($\mu = \frac{\Delta_{max}}{\Delta y}$) in Table 2 is defined by dividing the total displacement at the maximum load level (Δ_{max}) by the displacement at the elastic limit (Δ_y) [75]. To determine the yield displacement (Δ_y), the nonlinear pushover curve is approximated with an idealized bilinear curve, as described in FEMA 356 [72].

The structures were labeled using the notation S-t_A-M-σ_y, where t_A is the thickness of the metallic alloy, M is either steel (S) or aluminum (AL), and σ_y is the yielding strength of the metallic alloy. For instance, S10AL95 represents a two-layer lunar habitat in which the inner layer is made of aluminum with a thickness of 10 cm and a yielding strength of 95 MPa. Fragility curves and net present values were obtained for each structure to compare their performance over 20 years of service.

Table 2 Comparison between different system configurations

Structure (No.)	Ductility factor	Material A			Material B		
		Type	Yield stress (MPa)	Thickness (cm)	Type	Compression strength (MPa)	Thickness (cm)
S1AL95 (1)	1.40	Aluminum alloy 1100-H14	95.0	1.0	Regolith	25.0	120.0
S1AL230 (2)	1.42	Aluminum alloy 5456-H116	230.0	1.0	Regolith	25.0	120.0
S1AL500 (3)	1.79	Aluminum alloy 7075-T6	500.0	1.0	Regolith	25.0	120.0
S1S248 (4)	1.55	Steel A36	248.0	1.0	Regolith	25.0	120.0
S1S345 (5)	1.67	Steel A1085	345.0	1.0	Regolith	25.0	120.0
S1S483 (6)	1.91	Steel A913-70	483.0	1.0	Regolith	25.0	120.0
S3AL95 (7)	2.61	Aluminum alloy 1100-H14	95.0	3.0	Regolith	25.0	120.0
S3AL230 (8)	2.73	Aluminum alloy 5456-H116	230.0	3.0	Regolith	25.0	120.0
S3AL500 (9)	3.18	Aluminum alloy 7075-T6	500.0	3.0	Regolith	25.0	120.0
S3S248 (10)	3.06	Steel A36	248.0	3.0	Regolith	25.0	120.0
S3S345 (11)	3.62	Steel A1085	345.0	3.0	Regolith	25.0	120.0
S3S483 (12)	2.95	Steel A913-70	483.0	3.0	Regolith	25.0	120.0
S10AL95 (13)	2.11	Aluminum alloy 1100-H14	95.0	10.0	Regolith	25.0	120.0
S10AL230 (14)	2.02	Aluminum alloy 5456-H116	230.0	10.0	Regolith	25.0	120.0
S10AL500 (15)	2.49	Aluminum alloy 7075-T6	500.0	10.0	Regolith	25.0	120.0
S10S248 (16)	2.26	Steel A36	248.0	10.0	Regolith	25.0	120.0
S10S345 (17)	2.38	Steel A1085	345.0	10.0	Regolith	25.0	120.0
S10S483 (18)	2.61	Steel A913-70	483.0	10.0	Regolith	25.0	120.0

A. Fragility curves

Fragility curves were developed to estimate the probability of the structures experiencing failure or exceeding a damaged state over time. According to the conventional notion used in reliability theory [76], the limit state function was defined as:

$$g(t, \Delta) = C - \Delta(t) \tag{13}$$

where C indicates one of the LD limits and Δ is the lateral displacement of the structure due to external disturbances at any time, t. A structure exceeds or attains a performance level when $[g(t, \Delta) \leq 0]$. The fragility of the structural design is defined as:

$$F(t) = P\{[g(t, \Delta) \leq 0]|t\} \tag{14}$$

where $P\{[g(t, \Delta) \leq 0]$ denotes the conditional probability of reaching or exceeding a performance level, i.e., IO, LS, or CP, at a given time t.

The CDCM simulations are run at discrete time intervals (in the study, 24 hr time increments). Thus, to obtain continuous fragility estimates, a variety of well-known distribution functions (normal, lognormal, exponentiated Weibull, Weibull max, Weibull min, Pareto and beta) [77–79] were implemented to capture continuous fragility curves over t. The parameters for each distribution function were determined by fitting them on $F(t)$. The Kolmogorov-Smirnov goodness of fit test [80, 81] was applied to each distribution, and the p-value representing the likelihood of having two samples coming from the same distribution was computed. The distribution function with the highest p-value was chosen for computing each fragility curve.

B. Net Present Value (NPV)

To further illustrate the utility of having a habitat on the lunar surface, the NPV of various configurations are approximated. This was done by assuming that a functional lunar habitat is worth $v(X_t) = \$130,000$/hr of research when at state X_t [82]. The NPV of a design configuration (d) is estimated as below:

$$NPV(d) = \sum_{t=1}^{t_f} \beta^t \left(v(X_t) - C_{LC}(d)\right) - C_I(d) \tag{15}$$

where β is the discount factor computed according to the annual discount rate, λ, assumed as 5% in this study, C_I is the initial cost and C_{LC} is the life-cycle cost.

The initial cost for lunar habitat construction was estimated by computing the cost of sending metallic alloys from Earth to the lunar surface for every structure shown in Table 2. The initial cost estimates were calculated as follows,

$$C_I = M_A C_{trans} \tag{16}$$

where M_A stands for the mass of material A (structural layer) transported to the lunar surface and C_{trans} is the unit cost of sending mass to the Moon ($14,100/kg) via Falcon heavy [83–85]. The mass of material A was calculated as,

$$M_A = 2\pi R_{str}^2 t_A \rho_A \tag{17}$$

where t_A and ρ_A are the thickness and density of material A; and R_{str} is the radius of the dome.

The life-cycle cost, C_{LC}, was defined as the damage and repair cost resulting from micrometeorite impacts and moonquakes during the lifetime of the dome. This cost includes the resources used to repair damaged habitat components,

including structural and non-structural elements, and loss of contents [86]. This study estimated C_{LC} following Wen and Kang [87, 88] formulation, which approximates the life cycle cost as a percentage of C_I,

$$C_{LC} = \frac{1}{\lambda}(1 - e^{-\lambda t}) \sum_{i=1}^{7} C_I . MDI_i . P_i^p \tag{18}$$

where MDI_i is the mean damage index of the ith damage state as shown in Table 3; λ is the annual discount rate (5% in this study); P_i^p is the probability of passing damage state i, which is computed as

Table 3 Mean damage index and LD ratio for different damage states

Level No.	Damage state	Lateral drift ratio (%) [89]	Mean damage index (MDI) [90]
1	None	$LD_{max} \leq 0.1$	0.0
2	Slight	$0.1 < LD_{max} \leq 0.2$	0.005
3	Light	$0.2 < LD_{max} \leq 0.4$	0.05
4	Moderate	$0.4 < LD_{max} \leq 1.0$	0.2
5	Heavy	$1.0 < LD_{max} \leq 1.8$	0.45
6	Major	$1.8 < LD_{max} \leq 3.0$	0.80
7	Collapse	$3.0 < LD_{max}$	1.0

$$P_i^p = P(LD_{max} > LD_{max,i}) - P(LD_{max} > LD_{max,i+1}) \tag{19}$$

where $P(LD_{max} > LD_{max,i})$ is the violation probability of the designated LD at damage state i.

As the damage will vary for every realization conducted in the CDCM, the life cycle cost and the NPV will differ for every realization. Hence, the Expected Net Present Value (ENPV) and standard deviation (STD) of the NPV, RNPV, were also computed in the analysis.

IV. Results

Figure 10 shows the tip displacements for S3AL95 due to moonquakes and micrometeorite impacts during a life span of 20 years for a single realization. The residual displacement magnitudes over time are shown in Figure 11, where the curve jumps indicate those points in time in which the loading exceeded the yield strength of the material at time t and consequently induced additional plastic (unrecoverable) deformation to the structure. Following these instances, subsequent deformations are added to the residual displacement resulting from the previous time increment. Both plots show the influence of considering degradation due to temperature fluctuations. For this structural design, the residual displacement observed in the material-degraded structure was more than three times larger than that of the non-degraded structure. In addition, more jumps in plastic deformation were exhibited in the simulations considering material degradation.

To find the expected behavior of a structure, the simulations were repeated and the statistics of the realizations were computed until the STD and expected displacement converged to constant values. Figure 12 shows the tip

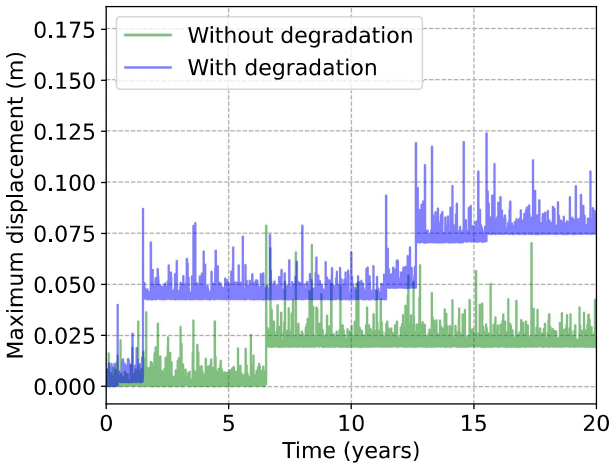

Fig. 10 Maximum displacement of S3AL95 as a result of moonquakes and micrometeorite impacts for a single realization.

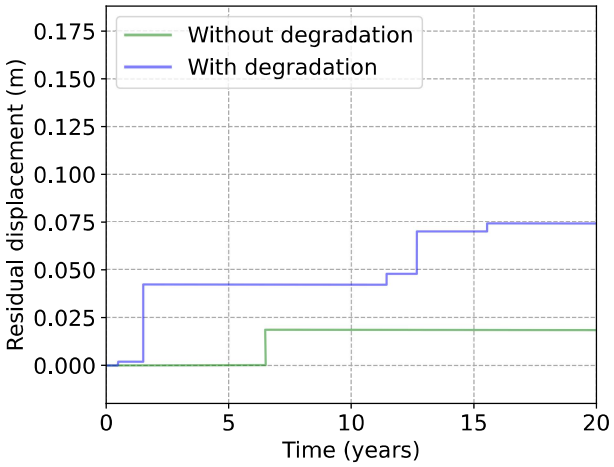

Fig. 11 Residual displacement of the structure as a result of moonquakes and micrometeorite impacts.

displacement for S3AL95 at 20 years for 100, 300, 500 and 600 realizations, showing that convergence was achieved at 600 realizations. Thus, all the structures described in Table 2 were subjected to 600 loading realizations to determine the average displacement behavior and its uncertainty.

The average maximum tip displacement curves for the eighteen structures are shown in Figure 13, where the band indicates one standard deviation above and below the mean value. S1AL500 experienced the highest average displacement, while S3S345 showed the lowest displacement after 20 years of sustained loading. The average and uncertainty of the residual displacement for each structure are also shown in Figure 13. S3S345 and S1AL500 were the structures with the highest and lowest average residual displacement, respectively. These results reveal that stiffer structures, such as S1AL95, tend to accumulate less plastic deformation but become unstable and show high displacements under sustained loading as time progresses. On the other hand, ductile structures, such as S3S345, tend

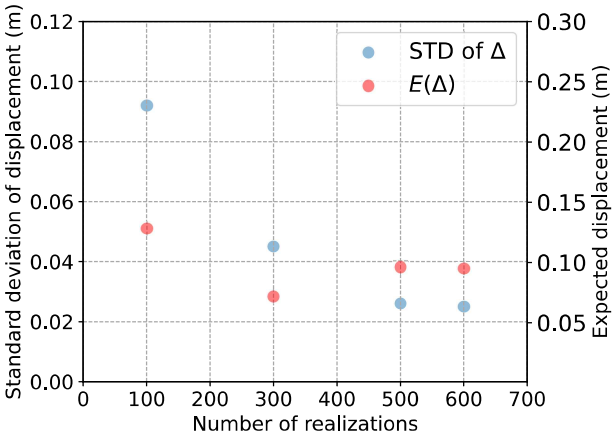

Fig. 12 Expected value and standard deviation of the roof displacement for S3AL95 after performing different numbers of realizations.

to accumulate more plastic deformation. However, as plastic deformation accumulates over time, the structures develop a damping mechanism that dissipates energy more efficiently than stiffer structures, as shown in Figure 13.

Fragility curves were obtained by evaluating the probability of reaching three predefined damage state levels (IO, LS, and CP) due to recurrent disturbances. Figure 14 illustrates the fragility curves for all 18 assembled lunar habitats. S3S345 has the lowest probability of collapse compared to the other structures; however, the IO has reached a probability of about 65% , indicating a high chance of requiring some rehabilitation after 20 years. The fragility curves illustrate that most structures are likely to experience damage that exceeds the IO level and, thus, require some kind of rehabilitation after 10 years of construction. The highest probability of reaching the CP state was observed in S1AL500 (94%), whereas S3S345 appeared to have a 6% chance of being on the verge of collapse after averaging the results of all conducted realizations. Another structure that showed a small probability of collapse was S3AL500. However, this structure exhibited a 77% possibility of reaching damage at the IO level at a 20-year lifespan.

Even though structures 13-18 were constructed out of metallic alloys with the highest thickness among all other structures, their performance did not significantly improve compared to thinner structures. This behavior was attributed to the introduction of unnecessary mass, which increased the force applied to these structures. In other words, increasing the thickness of the structures increased the structure's stiffness, which lowered its ductile capacity and ability to resist loading over extended periods.

The behavior of the stiff and ductile structures varies over time, as illustrated through the short and long-term performance comparison of S10AL95 and S3S345 in Figure 15. The structure with higher ductility, S3S345, with a ductility ratio of 3.6, has a higher slope than S10AL95, a structure with a ductility ratio 2.1, during the initial years of service. However, as time progresses, the less ductile structure (S10AL95 with a ductility ratio of 2.1) has a higher probability of reaching the LS and CP states. This behavior indicates that at the initial stages of service, the stiffer

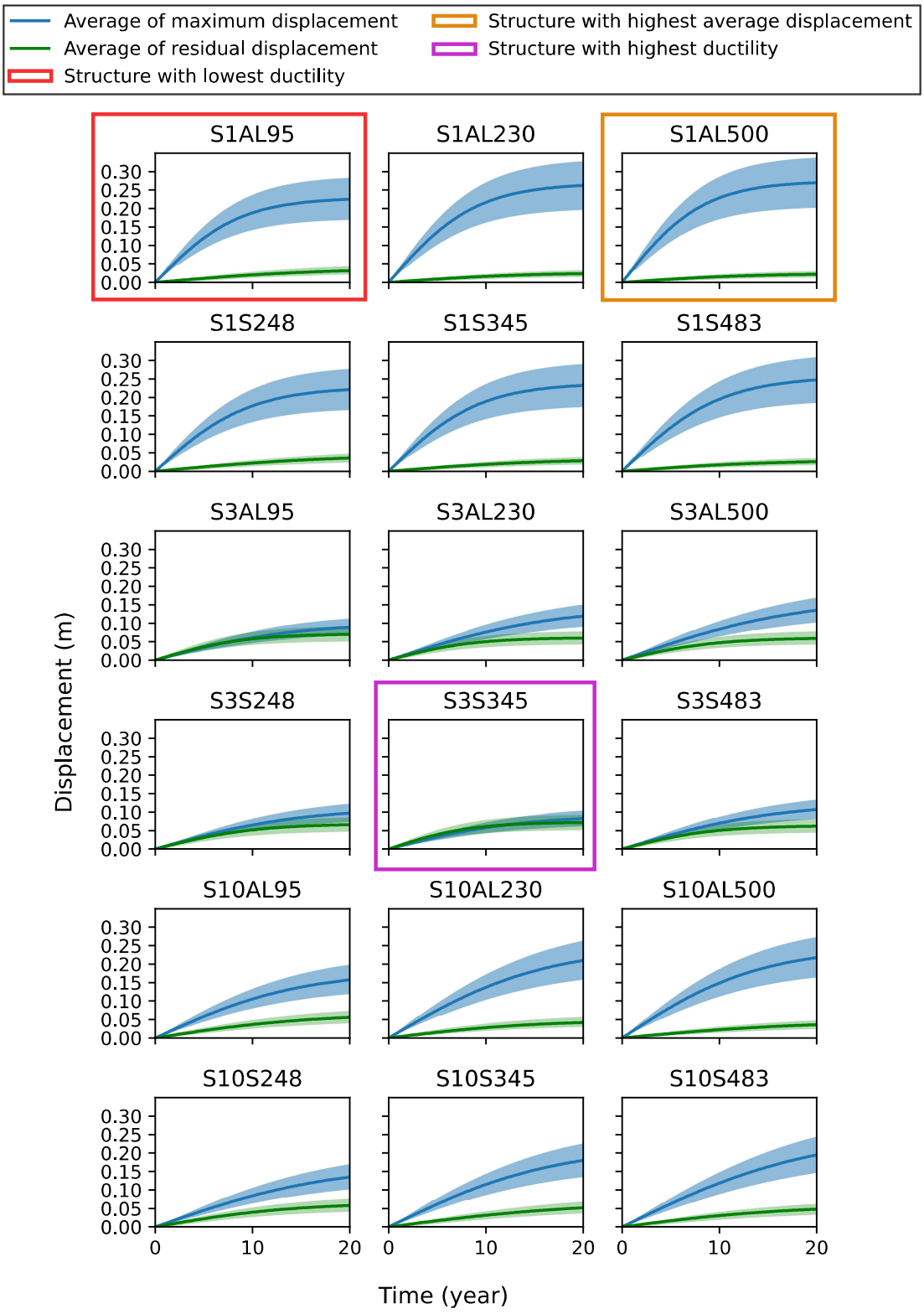

Fig. 13 Average of maximum and residual displacement for multiple realizations.

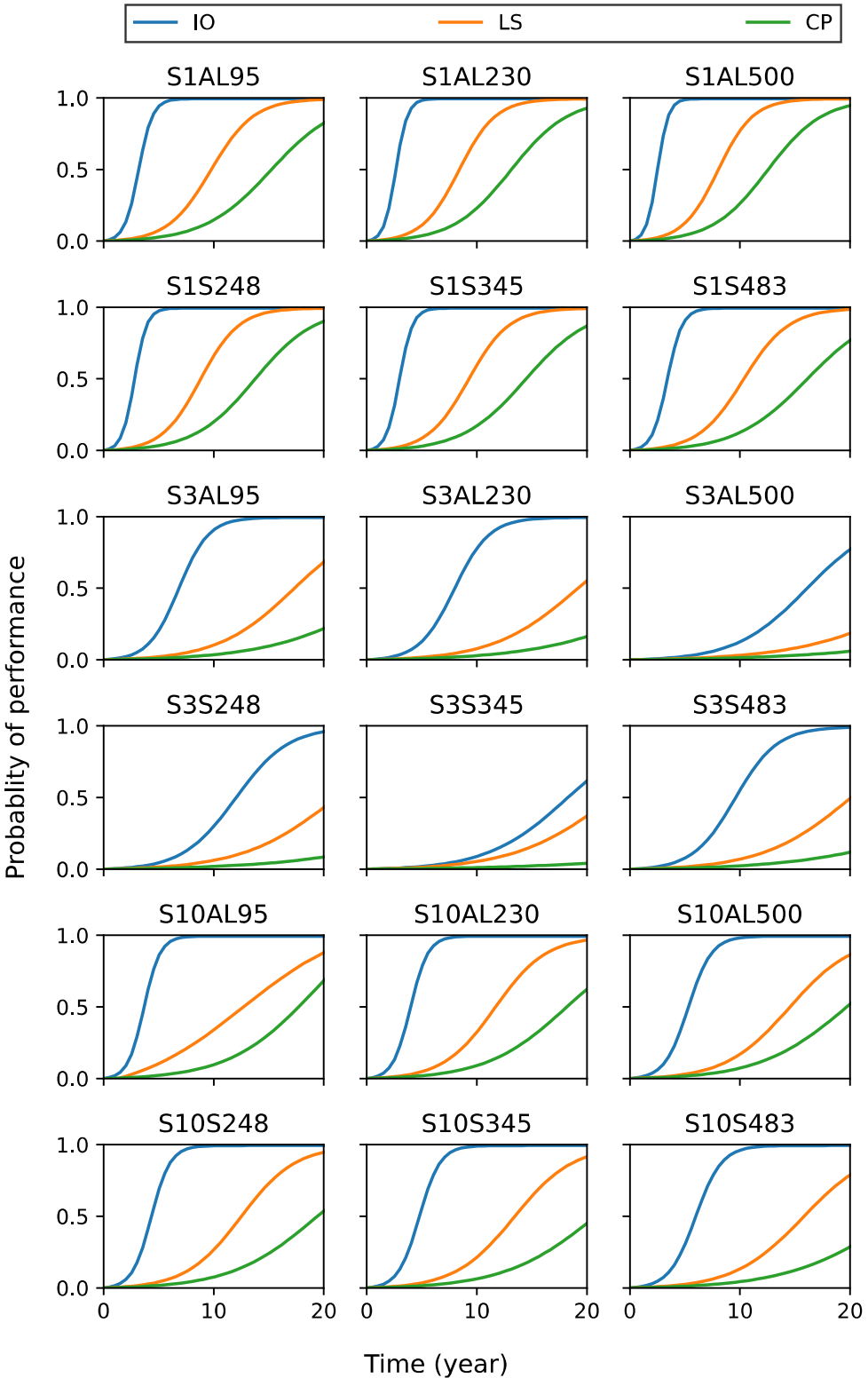

Fig. 14 Fragility curves for structures 1-18.

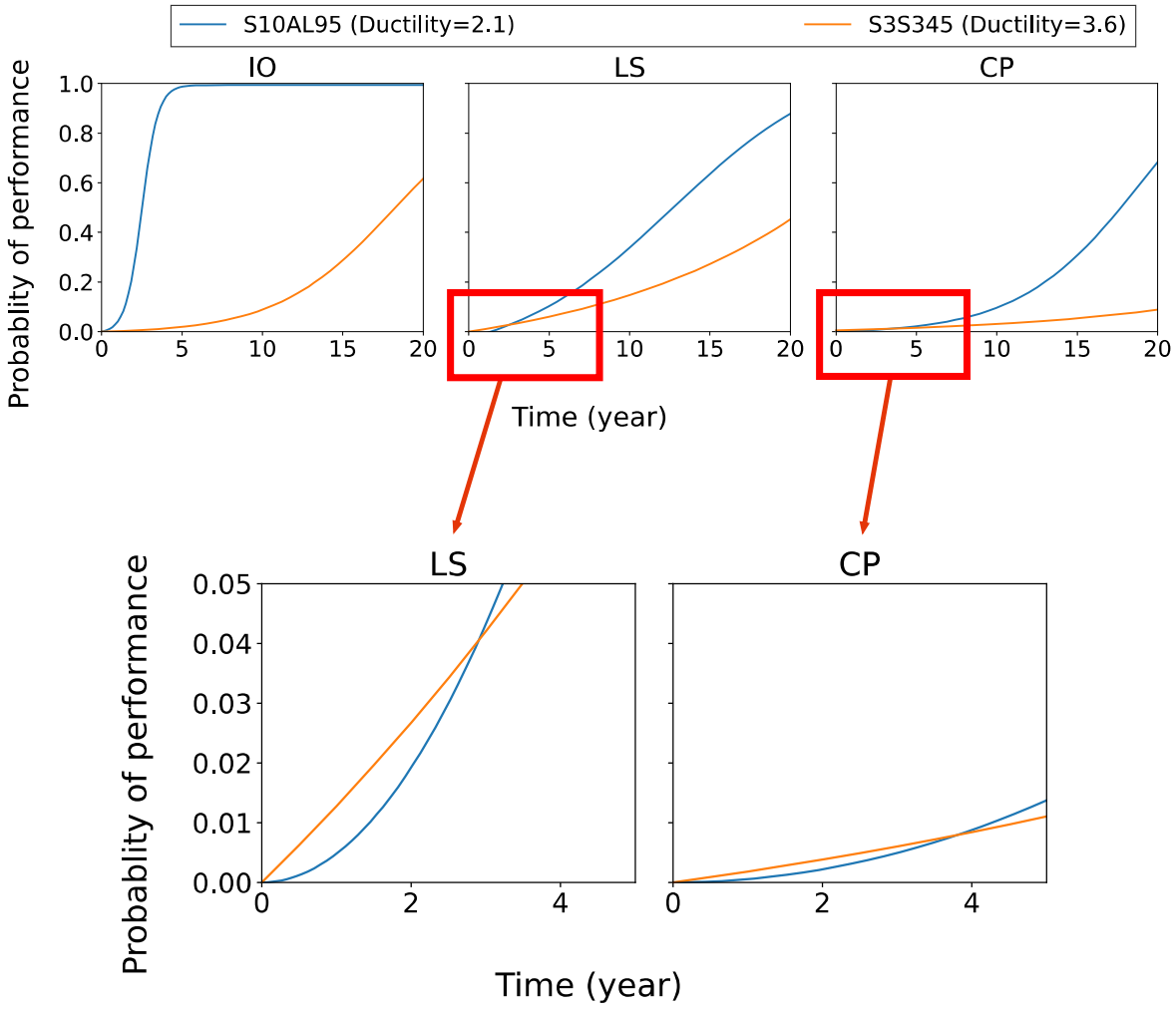

Fig. 15 Short and long-term fragility curves for S10AL95 and S3S345.

structures deform less, but as the damping mechanism due to plastic deformation develops within the ductile structures, they will deform more and have a higher risk of damage. The ductile structure shows higher resiliency in the long-term (for instance, 20 years), as they are more likely to reach the maximum allowed accumulated damage due to sustained loading over an extended period, minimizing major rehabilitation efforts.

The cost of structures 1-18 during a life-span of 20 years for a single realization are shown in Figure 16. The structures are listed in descending order with respect to ductility (ranging from 3.6 to 1.4). It is clear that the expected NPV for structures with lower ductility is less, which indicates that ductility plays an important role in the life cycle costs of a structure and, thus, in its NPV. This can also be observed in Figure 17, where the ENPV decreases in structures with lower ductility. Structures with a higher ductility factor have a lower RNPV, which indicates less variability in the structure's performance over time. Additionally, the probability of collapse for each structure versus their ENPV is depicted in Figure 18, in which structures with a lower probability of collapse in 20 years offer a higher ENPV.

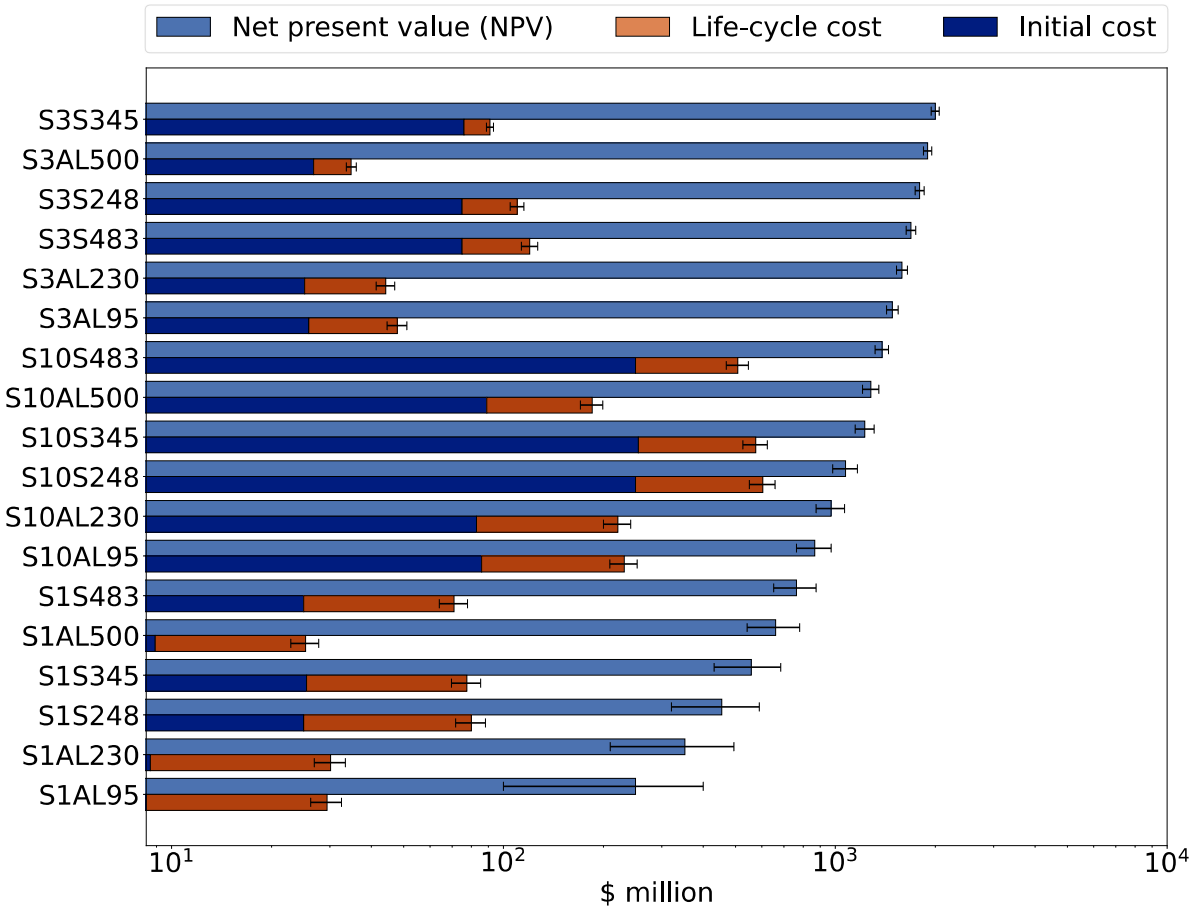

Fig. 16 ENPV, initial and life-cycle cost of structures 1-18.

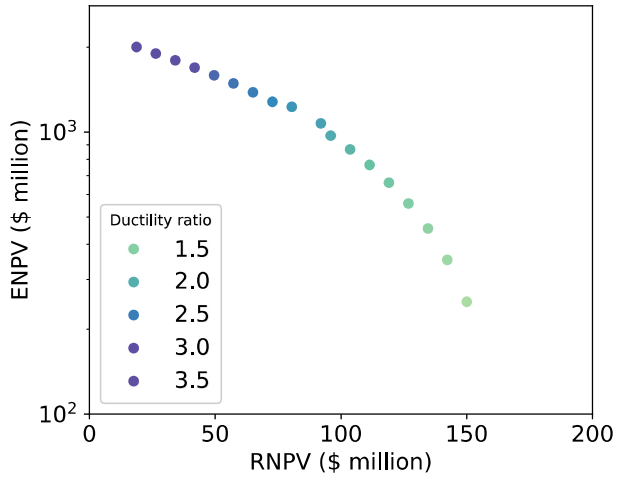

Fig. 17 ENPV vs RNPV for different ductility ratios.

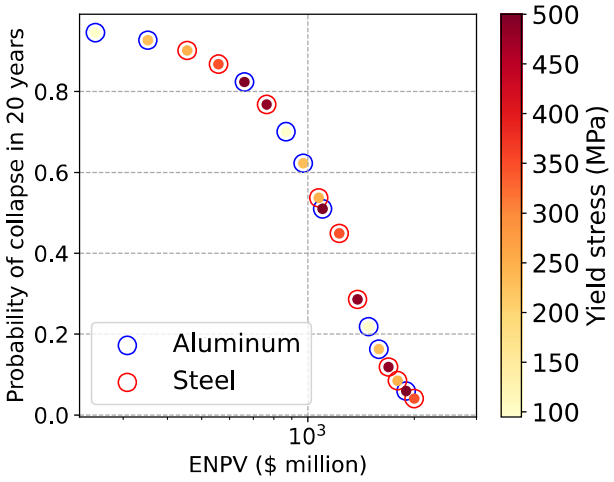

Fig. 18 The relationship between probability of collapse during a lifespan of 20 years and ENPV.

V. Discussion

The trade study indicates that ductility is important in keeping the habitat functional over a few decades. Ductility is also an important structural characteristic of Earth structures; however, it serves a different function. Structures with adequate ductility capacity on Earth survive extreme loading event scenarios with tolerable inelastic deformations. Buildings on Earth are always designed to save the lives of the occupants to stand after an extreme event, but most are not designed to still be used after that event. There are design codes established from decades of observations and experimental tests to protect lives. Decades of knowledge are used to design structures that withstand extreme lateral loads due to earthquakes, gust winds, or wave impacts. However, the structure might exploit its ductile capacity only once or twice during its lifetime.

On the other hand, lunar structures might experience smaller lateral loads, but some of these events, such as moonquakes, will last about 100 times longer because they do not dampen out. Micrometeorites will also hit the habitat and cause lateral deflections. Although more data collection is needed to characterize these loading scenarios fully, lunar habitats are anticipated to be subjected to recurrent disturbances from different loading sources. Ideally, preventive and corrective maintenance should be spaced out over time as resources will be limited in space. Ductile structures are able to keep damage within tolerable levels due to sustained loading for extended periods, reducing the probability of collapse. This behavior is attributed to the accumulation of permanent damage, which creates a damping mechanism that helps dissipate energy. In the case of metals, this damping mechanism is associated with the oscillation of dislocations. The energy from dislocations results in internal friction, which opposes lateral forces [91].

This trade study identifies an important structural characteristic that lunar habitats should possess; it is not the intent of this study to evaluate alternative designs available in the literature. The structural design was selected as it offered the flexibility of adjusting the ductile capacity of the conceptual design by varying its material and geometric

parameters. This design also facilitated developing an ROM that approximates the behavior of the structure within reasonable accuracy and executing multiple realizations using the CDCM. Within this paper, the model assumed fixed boundary conditions between the structure and lunar surface, which conditions the deflections of the structure; however, different types of structure-foundation connections have shown to alter the overall performance of the lunar habitat by altering the magnitude of stresses applied to the structure. Therefore, further analysis is required to determine potential connections between the structure and the lunar surface and ways to model it within the CDCM.

VI. Conclusion

In this study, a structural trade study using the CDCM and involving a variety of structures with different ductile capacities was performed to determine the influence of ductility on the performance of lunar habitats. The ductility of the structures was altered by varying the material properties and thickness of a monolithic dome structure covered by a regolith protective layer. The lunar habitat was assumed to have been constructed as the same location where the Apollo 17 program was performed. An ROM system representing the lateral behavior of a dome was modeled to capture the deflections caused as a result of moonquakes and micrometeorites impacts. High temperature fluctuations were assumed to degrade the material properties of the structural layer. Although the structural model has its own limitations, it provides a rapid and reasonable approximation of the long-term performance of lunar habitats. The displacement response due to the disturbances experienced over a life span of 20 years were used to assess the probability of each structure to reach the three damage states defined by FEMA 356. In addition, the ENPV for each of the 18 structures were computed to include a financial metrics that can be used to evaluate the use of resources invested in space habitats.

The trade study results revealed that at initial stages of the lunar habitat's lifespan, when high temperature fluctuations have not caused any significant material degradation, stiffer structures are less likely to suffer significant damage due to moonquake and micrometeorite impacts. However, under extended loading and under the presence of material degradation, ductile structures accumulate plastic deformation that generates a damping mechanism that provides better resistance against lateral deflections. According to these observations, ductility should become an important element in the design of space habitats, as it is likely that the maximum allowable damage will be experienced at a later stage in the service life of the structure. Hence, structural maintenance/repair actions can be delayed and limited resources can be utilized in other essential activities. In addition, according to the study, ductile structures had a higher ENPV and higher NPV/risk, providing a higher return on the initial investment.

The CDCM was a valuable tool for identifying features that would make structures resilient to disruptions and help guide space habitat design decisions. These insights are based on the limited understanding of the conditions and disturbances these habitats will face over an extended period of service in space. The analysis can be refined as more data is collected in space, and trade studies incorporate details related to surface characteristics, improve the characterization of the loading associated with moonquakes, micrometeorite impacts, and launch loads, and enhance the

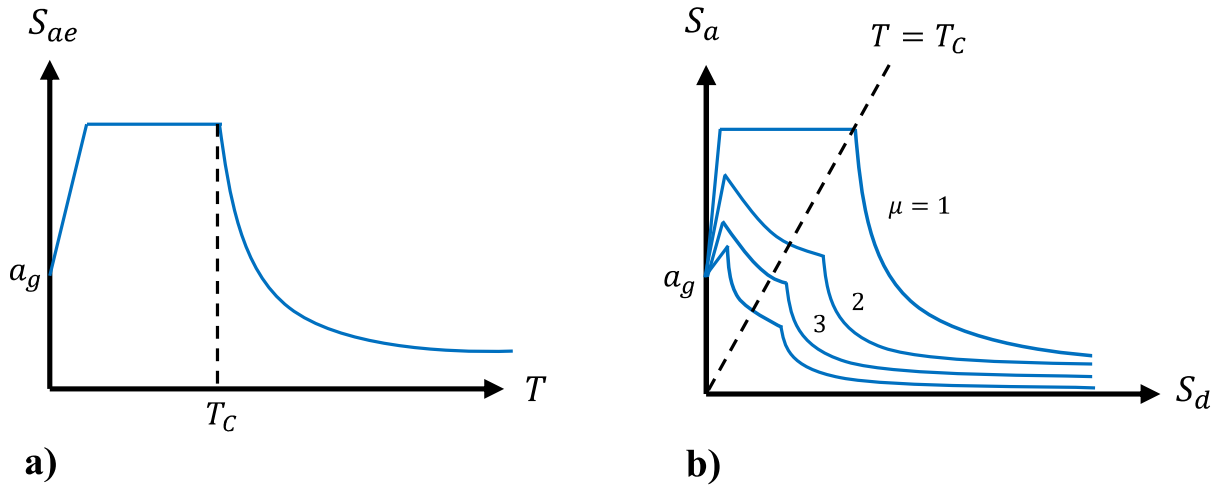

Fig. 19 Response spectrum: a) typical elastic acceleration (S_{ae}) spectrum; and b) demand spectra for constant ductilities in acceleration-displacement format.

material degradation mechanisms in space environments, among others.

Appendix

The displacement demand as a result of moonquakes on the structures were estimated by implementing the following steps:

a) Determine elastic spectra in Acceleration-Displacement (AD) format.

$$S_{de} = \frac{T^2}{4\pi^2} S_{ae} \tag{20}$$

where T is the period of the structure and S_{ae} is the value from the elastic acceleration spectrum, corresponding to the period T.

b) Determine inelastic spectra for constant ductilities.

$$R_\mu = \begin{cases} (\mu - 1)\frac{T}{T_c} + 1 & T < T_C \\ \mu & T \geq T_C \end{cases} \tag{21}$$

$$S_d = \frac{\mu}{R_\mu} S_{de} \tag{22}$$

where T_C is the characteristic period of the ground motion, μ is the ductility factor which is estimated using the pushover curve and S_d is the displacement demand. The above-mentioned estimations are shown in Figure 19.

Funding Sources

This study was based on research done under the Resilient Extra-Terrestrial Habitat Institute (RETHi) supported by a Space Technology Research Institute grant (No.80NSSC19K1076) from NASA's Space Technology Research Grants Program.

References

[1] Benaroya, H., "Lunar habitats: A brief overview of issues and concepts," *Reach*, Vol. 7, 2017, pp. 14–33. https://doi.org/10.1016/j.reach.2018.08.002.

[2] Ruess, F., Schaenzlin, J., and Benaroya, H., "Structural design of a lunar habitat," *Journal of Aerospace Engineering*, Vol. 19, No. 3, 2006, pp. 133–157.

[3] Benaroya, H., Bernold, L., and Chua, K. M., "Engineering, design and construction of lunar bases," *Journal of Aerospace Engineering*, Vol. 15, No. 2, 2002, pp. 33–45. https://doi.org/10.1007/978-3-319-68244-0_8.

[4] Jolly, S. D., Happel, J., and Sture, S., "Design and construction of shielded lunar outpost," *Journal of Aerospace Engineering*, Vol. 7, No. 4, 1994, pp. 417–434. https://doi.org/10.1061/(asce)0893-1321(1994)7:4(417).

[5] Belvin, W., Watson, J., and Singhal, S., "Structural concepts and materials for lunar exploration habitats," *Space 2006*, 2006, p. 7338. https://doi.org/10.2514/6.2006-7338.

[6] Park, J., Montoya, H., Fu, Y., Maghareh, A., Dyke, S. J., and Ziviani, D., "Development of a Virtual Cyber-Physical Testbed for Resilient Extraterrestrial Habitats," *Thermal and Fluids Analysis Workshop*, 2021.

[7] Degtyarev, A., Kushnar'ov, O., Baranov, E., Osinovyy, G., Lysenko, J., and Kaliapin, M., "Minimal Configuration Lunar Habitat," *2018 SpaceOps Conference*, 2018, p. 2380. https://doi.org/10.2514/6.2018-2380.

[8] Lynch, C., Stromgren, C., Cirillo, W., Owens, A., Drake, B. G., and Beaton, K., "Early Assessments of Crew Timelines for the Lunar Surface Habitat," *ASCEND 2022*, 2022, p. 4236. https://doi.org/10.2514/6.2022-4236.

[9] Fu, K., Du, J., Li, J., and Zhao, Z., "Robust design of tension truss antennas against variation in tension forces," *AIAA Journal*, Vol. 56, No. 8, 2018, pp. 3374–3381. https://doi.org/10.2514/1.j056461.

[10] Dai, L., and Hu, L., "Kinematic Analysis and Model Fabrication of a Space Deployable Optical Baffle," *AIAA Journal*, Vol. 58, No. 3, 2020, pp. 1386–1396. https://doi.org/10.2514/1.j058829.

[11] Otsuka, K., and Makihara, K., "Absolute nodal coordinate beam element for modeling flexible and deployable aerospace structures," *AIAA journal*, Vol. 57, No. 3, 2019, pp. 1343–1346. https://doi.org/10.2514/1.j057780.

[12] Shahriar, A., Majlesi, A., and Montoya, A., "A General Procedure to Formulate 3D Elements for Finite Element Applications," *Computation*, Vol. 11, No. 10, 2023, p. 197. https://doi.org/10.3390/computation11100197.

[13] Suggs, R., and Suggs, R. M., "Results of Lunar Impact Observations During Geminid Meteor Shower Events," Tech. rep., 2015.

[14] Grün, E., Zook, H. A., Fechtig, H., and Giese, R., "Collisional balance of the meteoritic complex," *Icarus*, Vol. 62, No. 2, 1985, pp. 244–272. https://doi.org/10.1016/0019-1035(85)90121-6.

[15] Jones, H. W., "Space Habitats Should Be 1 g Shielded Space Platforms, Not on Low Gravity, Radiation Exposed Moon or Mars," *INCOSE International Symposium*, Vol. 32, Wiley Online Library, 2022, pp. 390–402. https://doi.org/10.1002/iis2.12938.

[16] Baker, J., and Heyman, J., *Plastic design of frames 1 fundamentals*, Cambridge University Press, 1969. https://doi.org/10.1017/cbo9780511586514.004.

[17] Housner, G. W., and Wiegel, R., *Earthquake engineering*, 1970.

[18] Ghorbani, R., Suselo, A., Gendy, S., Matamoros, A., and Ghannoum, W., "Uniaxial model for simulating the cyclic behavior of reinforced concrete members," *Earthquake Engineering & Structural Dynamics*, Vol. 51, No. 15, 2022, pp. 3574–3597. https://doi.org/https://doi.org/10.1002/eqe.3736.

[19] Park, R., "Ductile design approach for reinforced concrete frames," *Earthquake spectra*, Vol. 2, No. 3, 1986, pp. 565–619. https://doi.org/10.1193/1.1585398.

[20] Paulay, T., "The design of ductile reinforced concrete structural walls for earthquake resistance," *Earthquake Spectra*, Vol. 2, No. 4, 1986, pp. 783–823. https://doi.org/10.1193/1.1585411.

[21] Nunn, C., Garcia, R. F., Nakamura, Y., Marusiak, A. G., Kawamura, T., Sun, D., Margerin, L., Weber, R., Drilleau, M., Wieczorek, M. A., et al., "Lunar seismology: A data and instrumentation review," *Space Science Reviews*, Vol. 216, No. 5, 2020, pp. 1–39. https://doi.org/10.1007/s11214-020-00709-3.

[22] Nakamura, Y., Latham, G. V., and Dorman, H. J., "Apollo lunar seismic experiment—Final summary," *Journal of Geophysical Research: Solid Earth*, Vol. 87, No. S01, 1982, pp. A117–A123. https://doi.org/10.1029/jb087is01p0a117.

[23] Khan, A., and Mosegaard, K., "An inquiry into the lunar interior: A nonlinear inversion of the Apollo lunar seismic data," *Journal of Geophysical Research: Planets*, Vol. 107, No. E6, 2002, pp. 3–1. https://doi.org/10.1029/2001je001658.

[24] Nakamura, Y., "Shallow moonquakes-How they compare with earthquakes," *Lunar and Planetary Science Conference Proceedings*, Vol. 11, 1980, pp. 1847–1853.

[25] Nakamura, Y., Latham, G. V., Dorman, H. J., Ibrahim, A.-B., Koyama, J., and Horvath, P., "Shallow moonquakes-depth, distribution and implications as to the present state of the lunar interior," *Lunar and Planetary Science Conference Proceedings*, Vol. 10, 1979, pp. 2299–2309.

[26] Ruiz, S., Cruz, A., Gomez, D., Dyke, S. J., and Ramirez, J., "Preliminary approach to assess the seismic hazard on a lunar site," *Icarus*, Vol. 383, 2022, p. 115056. https://doi.org/10.1016/j.icarus.2022.115056.

[27] Oberst, J., "Unusually high stress drops associated with shallow moonquakes," *Journal of Geophysical Research: Solid Earth*, Vol. 92, No. B2, 1987, pp. 1397–1405. https://doi.org/10.1029/jb092ib02p01397.

[28] Oberst, J., and Nakamura, Y., "A seismic risk for the lunar base," *NASA. Johnson Space Center, The Second Conference on Lunar Bases and Space Activities of the 21st Century, Volume 1*, 1992.

[29] Watters, T., Weber, R., Collins, G., Howley, I., Schmerr, N., and Johnson, C., "Shallow seismic activity and young thrust faults on the Moon Nat," , 2019. https://doi.org/10.1038/s41561-019-0362-2.

[30] Montoya, H. P., Dyke, S., Ramirez, J. A., Bobet, A., Melosh, H. J., and Gomez, D., "Hazard Assessment of Meteoroid Impact for the Design of Lunar Habitats," 2017.

[31] Balakrishnan, K., and Bellan, J., "Ejecta from Granular-Medium Cratering by a Supersonic Jet Entering a Continuum Atmosphere," *AIAA Journal*, Vol. 59, No. 10, 2021, pp. 3799–3814. https://doi.org/10.2514/1.j060563.

[32] French, B. M., Heiken, G., Vaniman, D., Schmitt, H. H., and Schmitt, J., *Lunar sourcebook: A user's guide to the Moon*, 1259, CUP Archive, 1991. https://doi.org/10.1016/0160-9327(92)90014-g.

[33] Moorhead, A., Koehler, H., and Cooke, W., "NASA meteoroid engineering model release 2.0," Tech. rep., 2015.

[34] Montoya, H., Dyke, S. J., Silva, C. E., Maghareh, A., Park, J., and Ziviani, D., "Thermomechanical Real-Time Hybrid Simulation: Conceptual Framework and Control Requirements," *AIAA Journal*, Vol. 61, No. 6, 2023, pp. 2627–2639. https://doi.org/10.2514/1.j062857.

[35] Dennis, H. J., and Componation, P. J., "An Examination of the Trade Study Process at NASA," *Engineering Management Journal*, Vol. 16, No. 4, 2004, pp. 10–18. https://doi.org/10.1080/10429247.2004.11415261.

[36] NASA, S., "Nasa systems engineering handbook," *National Aeronautics and Space Administration, NASA/SP-2007-6105 Rev1*, 2007.

[37] Lightsey, B., "Systems engineering fundamentals," Tech. rep., DEFENSE ACQUISITION UNIV FT BELVOIR VA, 2001.

[38] Lee, J. A., Carini, J., Choi, A., Dillman, R., Griffin, S. J., Hanneman, S., Mamplata, C., and Stanton, E., "Lunar lander conceptual design," Tech. rep., 1989.

[39] Dezfuli, H., Stamatelatos, M., Maggio, G., Everett, C., Youngblood, R., Rutledge, P., Benjamin, A., Williams, R., Smith, C., and Guarro, S., "NASA risk-informed decision making handbook," Tech. rep., 2010.

[40] Team, E. S. A. S., et al., "Exploration Systems Architecture Study-Final Report," , 2005.

[41] Hirshorn, S. R., Voss, L. D., and Bromley, L. K., "Nasa systems engineering handbook," Tech. rep., 2017.

[42] Behjat, A., Ibrahimov, R., Lenjani, A., Barket, A., Martinus, K., Maghareh, A., Whitaker, D., Bilionis, I., and Dyke, S., "A Computational Framework for the Evaluation of Resilience in Deep Space Habitat Systems," *International Design Engineering*

Technical Conferences and Computers and Information in Engineering Conference, Vol. 86229, American Society of Mechanical Engineers, 2022, p. V03AT03A036. https://doi.org/10.1115/detc2022-89132.

[43] Behjat, A., Liu, X., Foreco, O., Ibrahimov, R., Dyke, S. J., Bilionis, I., Ramirez, J., and Whitaker, D., "A Computational Framework for Making Early Design Decisions in Deep Space Habitats," *Advances in Engineering Software*, 2024. (in reviewe).

[44] Liu, X., Behjat, A., Dyke, S., Whitaker, D., Ramirez, J., and Bilionis, I., "Roles of Human and Robotic Agents Toward Operating a Smart Space Habitat," 2023 International Conference on Environmental Systems, 2023.

[45] Sansoucie, M. P., hull, P. V., and Tinker, M. L., "Habitat design optimization and analysis," 2006. https://doi.org/10.3727/154296610x12686999887364.

[46] Zook, H. A., "The state of meteoritic material on the Moon," *Lunar and Planetary Science Conference Proceedings*, Vol. 6, 1975, pp. 1653–1672.

[47] Valentin, J., *The 2007 recommendations of the international commission on radiological protection*, Elsevier International Commission on Radiological Protection, 2008.

[48] Warner, C. M., "Lunar Living: NASA's Artemis Base Camp Concept," , 2020. URL https://blogs.nasa.gov/artemis/2020/10/28/lunar-living-nasas-artemis-base-camp-concept.

[49] Singleterry Jr, R. C., Blattnig, S. R., Clowdsley, M. S., Qualls, G. D., Sandridge, C. A., Simonsen, L. C., Slaba, T. C., Walker, S. A., Badavi, F. F., Spangler, J. L., et al., "OLTARIS: On-line tool for the assessment of radiation in space," *Acta Astronautica*, Vol. 68, No. 7-8, 2011, pp. 1086–1097. https://doi.org/10.2514/6.2009-6645.

[50] "On-Line Tool for the Assessment of Radiation ins Space," https://oltaris.nasa.gov, 2022.

[51] Adams, J. H., Barghouty, N., Bhattacharya, M., and Lin, Z.-W., "Radiation Shielding: Lunar Simulant Requirements," 2005. URL https://www.nasa.gov/wp-content/uploads/2019/04/radiation_shielding.pdf.

[52] Slaba, T. C., "Radiation Shielding for Lunar Missions: Regolith Considerations," *LSIC Crosstalk*, 2022. URL https://lsic.jhuapl.edu/uploadedDocs/focus-files.

[53] Wilson, J., Kim, M., Schimmerling, W., Badavi, F., Thibeault, S., Cucinotta, F., Shinn, L., and Kiefer, R., "Issues in space radiation protection: galactic cosmic rays," *Health Physics*, Vol. 68, No. 1, 1995, pp. 50–58. https://doi.org/10.1097/00004032-199501000-00006.

[54] Parnell, T. A., Watts, J. W., Jr, and Armstrong, T. W., "Radiation effects and protection for moon and mars missions," *Space 98*, 1998, pp. 232–244. https://doi.org/10.1061/40339(206)28.

[55] Xapsos, M. A., Burke, E. A., Shapiro, P., and Summers, G. P., "Energy deposition and ionization fluctuations induced by ions in small sites: An analytical approach," *Radiation research*, Vol. 137, No. 2, 1994, pp. 152–161. https://doi.org/10.2307/3578806.

[56] Xapsos, M. A., Burke, E. A., Shapiro, P., and Summers, G. P., "Probability distributions of energy deposition and ionization in sub-micrometer sites of condensed media," *Radiation measurements*, Vol. 26, No. 1, 1996, pp. 1–9. https://doi.org/10.1016/1350-4487(95)00296-0.

[57] Allende, M. I., Miller, J. E., Davis, B. A., Christiansen, E. L., Lepech, M. D., and Loftus, D. J., "Prediction of micrometeoroid damage to lunar construction materials using numerical modeling of hypervelocity impact events," *International Journal of Impact Engineering*, Vol. 138, 2020, p. 103499. https://doi.org/10.1115/hvis2019-036.

[58] Mazzoni, S., McKenna, F., Scott, M. H., Fenves, G. L., et al., "OpenSees command language manual," *Pacific Earthquake Engineering Research (PEER) Center*, Vol. 264, No. 1, 2006, pp. 137–158.

[59] Zhu, M., McKenna, F., and Scott, M. H., "OpenSeesPy: Python library for the OpenSees finite element framework," *SoftwareX*, Vol. 7, 2018, pp. 6–11. https://doi.org/10.1016/j.softx.2017.10.009.

[60] Ruangrassamee, A., and Kawashima, K., "Control of nonlinear bridge response with pounding effect by variable dampers," *Engineering Structures*, Vol. 25, No. 5, 2003, pp. 593–606. https://doi.org/10.1016/s0141-0296(02)00169-4.

[61] Abaqus, G., "Abaqus 6.11," *Dassault Systemes Simulia Corporation, Providence, RI, USA*, 2011.

[62] Fajfar, P., "A nonlinear analysis method for performance-based seismic design," *Earthquake spectra*, Vol. 16, No. 3, 2000, pp. 573–592. https://doi.org/10.1193/1.1586128.

[63] Kang, J.-H., "Free vibration analysis of shallow spherical dome by three-dimensional Ritz method," *Journal of Vibration and Control*, Vol. 22, No. 11, 2016, pp. 2731–2744. https://doi.org/10.1177/1077546314551446.

[64] McGee, O., and Spry, S., "A THREE-DIMENSIONAL ANALYSIS OF THE SPHEROIDAL AND TOROIDAL ELASTIC VIBRATIONS OF THICK-WALLED SPHERICAL BODIES OF REVOLUTION," *International journal for numerical methods in engineering*, Vol. 40, No. 8, 1997, pp. 1359–1382.

[65] Zhang, Q., Wang, Z., Tang, C. Y., Hu, D., Liu, P., and Xia, L., "Analytical solution of the thermo-mechanical stresses in a multilayered composite pressure vessel considering the influence of the closed ends," *International Journal of Pressure Vessels and Piping*, Vol. 98, 2012, pp. 102–110. https://doi.org/10.1016/j.ijpvp.2012.07.009.

[66] Parsapoor, A., Whittington, A., Majlesi, A., Giberga, O., Wells, R., and Ximenes, S., "Effect of Cooling Rate on the Microstructure of Crystallizing LCATS-1 Lunar Regolith Simulant," *LPI Contributions*, Vol. 2678, 2022, p. 2824.

[67] Hoła, J., "Experimentally determined effects of technological and service factors on stress-induced destruction of concrete under compression," *Engineering Transactions*, Vol. 50, No. 4, 2002, pp. 251–265. https://doi.org/10.24423/engtrans.531.2002.

[68] Bamshad, O., Mahdikhani, M., Ramezanianpour, A. M., Maleki, Z., Majlesi, A., Habibi, A., and Delavar, M. A., "Prediction and multi-objective optimization of workability and compressive strength of recycled self-consolidating mortar using Taguchi design method," *Heliyon*, Vol. 9, No. 6, 2023. https://doi.org/10.2139/ssrn.4346720.

[69] Morrow, J., "Fatigue properties of metals," *Fatigue design handbook*, Vol. 4, 1968, pp. 21–30.

[70] Dowling, N., "Mechanical Behavior of Materials. Fourt edition," , 2013.

[71] Schijve, J., *Fatigue of structures and materials*, Springer, 2009.

[72] FEMA, "Prestandard and commentary for the seismic rehabilitation of buildings (FEMA356)," *Washington, DC: Federal Emergency Management Agency*, Vol. 7, No. 2, 2000.

[73] Koodiani, H. K., Majlesi, A., Shahriar, A., and Matamoros, A., "Non-linear modeling parameters for new construction RC columns. Front," *Built Environ*, Vol. 9, 2023, p. 1108319. https://doi.org/10.3389/fbuil.2023.1108319.

[74] Morales-González, M., and Vidot-Vega, A. L., "Seismic response of reinforced concrete frames at different damage levels," *International Journal of Advanced Structural Engineering*, Vol. 9, 2017, pp. 63–77. https://doi.org/10.1007/s40091-017-0149-x.

[75] Gholipour, M., and Alinia, M. M., "Considereation on the pushover analysis of multi-story steel plate shear wall structures," *Periodica Polytechnica Civil Engineering*, Vol. 60, No. 1, 2016, pp. 113–126. https://doi.org/10.3311/ppci.7706.

[76] Ramamoorthy, S. K., Gardoni, P., and Bracci, J. M., "Probabilistic demand models and fragility curves for reinforced concrete frames," *Journal of structural Engineering*, Vol. 132, No. 10, 2006, pp. 1563–1572. https://doi.org/10.1061/(asce)0733-9445(2006)132:10(1563).

[77] Bali, T. G., "The generalized extreme value distribution," *Economics letters*, Vol. 79, No. 3, 2003, pp. 423–427. https://doi.org/10.1016/S0165-1765(03)00035-1.

[78] Arnold, B. C., "Pareto distribution," *Wiley StatsRef: Statistics Reference Online*, 2014, pp. 1–10. https://doi.org/10.1002/9781118445112.stat01100.pub2.

[79] McLaughlin, M. P., *A compendium of common probability distributions*, Michael P. McLaughlin, 2001.

[80] Massey Jr, F. J., "The Kolmogorov-Smirnov test for goodness of fit," *Journal of the American statistical Association*, Vol. 46, No. 253, 1951, pp. 68–78.

[81] Miller, L. H., "Table of percentage points of Kolmogorov statistics," *Journal of the American Statistical Association*, Vol. 51, No. 273, 1956, pp. 111–121. https://doi.org/10.1080/01621459.1956.10501314.

[82] Foust, J., "NASA hikes prices for commercial ISS users," , 2021. URL https://spacenews.com/nasa-hikes-prices-for-commercial-iss-users/.

[83] Jones, H., "The recent large reduction in space launch cost," 48th International Conference on Environmental Systems, 2018.

[84] Hinkle, J., Timmers, R., Dixit, A., Lin, J., and Watson, J., "Structural design, analysis, and testing of an expandable lunar habitat," *50th AIAA/ASME/ASCE/AHS/ASC Structures, Structural Dynamics, and Materials Conference 17th AIAA/ASME/AHS Adaptive Structures Conference 11th AIAA No*, 2009, p. 2166. https://doi.org/10.2514/6.2009-2166.

[85] Carson, J. M., Munk, M. M., and Wright, M. J., "NASA development strategy for navigation technologies to precisely land payloads and avoid landing hazards," *AIAA SCITECH 2022 Forum*, 2022, p. 0355. https://doi.org/10.2514/6.2022-0355.

[86] Fragiadakis, M., Lagaros, N. D., and Papadrakakis, M., "Performance-based multiobjective optimum design of steel structures considering life-cycle cost," *Structural and Multidisciplinary Optimization*, Vol. 32, 2006, pp. 1–11. https://doi.org/10.1007/s00158-006-0009-y.

[87] Wen, Y.-K., and Kang, Y., "Minimum building life-cycle cost design criteria. I: Methodology," *Journal of Structural Engineering*, Vol. 127, No. 3, 2001, pp. 330–337. https://doi.org/10.1061/(asce)0733-9445(2001)127:3(330).

[88] Wen, Y., and Kang, Y., "Minimum building life-cycle cost design criteria. II: Applications," *Journal of Structural Engineering*, Vol. 127, No. 3, 2001, pp. 338–346. https://doi.org/10.1061/(asce)0733-9445(2001)127:3(338).

[89] Ghobarah, A., "On drift limits associated with different damage levels," *International workshop on performance-based seismic design*, Vol. 28, Department of Civil Engineering, McMaster University Ontario, Canada, 2004.

[90] 227, F., "A benefit–cost model for the seismic rehabilitation of buildings," , 1992.

[91] Jones, R. L., *A constitutive relationship between crack propagation and specific damping capacity in steel*, Naval Civil Engineering Laboratory, 1990.